



UvA-DARE (Digital Academic Repository)

Orbital-exchange and fractional quantum number excitations in an f-electron metal, $\text{Yb}_2\text{Pt}_2\text{Pb}$

Wu, L.S.; Gannon, W.J.; Zaliznyak, I.A.; Tsvelik, A.M.; Brockmann, M.; Caux, J.-S.; Kim, M.S.; Qiu, Y.; Copley, J.R.D.; Ehlers, G.; Podlesnyak, A.; Aronson, M.C.

DOI

[10.1126/science.aaf0981](https://doi.org/10.1126/science.aaf0981)

Publication date

2016

Document Version

Final published version

Published in

Science

License

Article 25fa Dutch Copyright Act (<https://www.openaccess.nl/en/in-the-netherlands/you-share-we-take-care>)

[Link to publication](#)

Citation for published version (APA):

Wu, L. S., Gannon, W. J., Zaliznyak, I. A., Tsvelik, A. M., Brockmann, M., Caux, J.-S., Kim, M. S., Qiu, Y., Copley, J. R. D., Ehlers, G., Podlesnyak, A., & Aronson, M. C. (2016). Orbital-exchange and fractional quantum number excitations in an f-electron metal, $\text{Yb}_2\text{Pt}_2\text{Pb}$. *Science*, 352(6290), 1206-1210. <https://doi.org/10.1126/science.aaf0981>

General rights

It is not permitted to download or to forward/distribute the text or part of it without the consent of the author(s) and/or copyright holder(s), other than for strictly personal, individual use, unless the work is under an open content license (like Creative Commons).

Disclaimer/Complaints regulations

If you believe that digital publication of certain material infringes any of your rights or (privacy) interests, please let the Library know, stating your reasons. In case of a legitimate complaint, the Library will make the material inaccessible and/or remove it from the website. Please Ask the Library: <https://uba.uva.nl/en/contact>, or a letter to: Library of the University of Amsterdam, Secretariat, Singel 425, 1012 WP Amsterdam, The Netherlands. You will be contacted as soon as possible.

UvA-DARE is a service provided by the Library of the University of Amsterdam (<https://dare.uva.nl>)

Orbital-exchange and fractional quantum number excitations in an f-electron metal, Yb₂Pt₂Pb

L. S. Wu,^{1,2,3} W. J. Gannon,^{1,2,4} I. A. Zaliznyak,^{2*} A. M. Tselvik,² M. Brockmann,^{5,6} J.-S. Caux,⁶ M. S. Kim,² Y. Qiu,⁷ J. R. D. Copley,⁷ G. Ehlers,³ A. Podlesnyak,³ M. C. Aronson^{1,2,4}

Exotic quantum states and fractionalized magnetic excitations, such as spinons in one-dimensional chains, are generally expected to occur in 3d transition metal systems with spin 1/2. Our neutron-scattering experiments on the 4f-electron metal Yb₂Pt₂Pb overturn this conventional wisdom. We observe broad magnetic continuum dispersing in only one direction, which indicates that the underlying elementary excitations are spinons carrying fractional spin-1/2. These spinons are the emergent quantum dynamics of the anisotropic, orbital-dominated Yb moments. Owing to their unusual origin, only longitudinal spin fluctuations are measurable, whereas the transverse excitations such as spin waves are virtually invisible to magnetic neutron scattering. The proliferation of these orbital spinons strips the electrons of their orbital identity, resulting in charge-orbital separation.

It is generally believed that fractional quantum excitations such as spinons in one-dimensional (1D) spin chains proliferate and govern magnetism only in systems with small and isotropic atomic magnetic moments, such as spin-1/2 Cu²⁺. In contrast, large and anisotropic orbital-dominated moments, such as those produced by strong spin-orbit coupling in the rare

earths, are considered to be classical, becoming static as temperature $T \rightarrow 0$ because the conventional Heisenberg-Dirac exchange interaction (1, 2) cannot reverse their directions. Here we present the results of neutron-scattering measurements on the 3D compound Yb₂Pt₂Pb that profoundly challenge this conventional wisdom.

The unusual properties of Yb₂Pt₂Pb derive in part from its crystal structure (Fig. 1, A and B), where the Yb³⁺ ions form ladders along the *c* axis, separated by Pt and Pb; the rungs of the ladders (dashed lines in Fig. 1A) lie on the orthogonal bonds of the Shastry-Sutherland lattice (SSL) (3) in the *ab* planes. Equally important is the strong spin-orbit coupling, which combines spin and orbital degrees of freedom into a large, $J = 7/2$ Yb moment. The absence of a Kondo effect indicates minimal coupling of Yb to the conduction electrons of this excellent metal (4, 5). A point-charge model (6) indicates that the crystal electric field (CEF) lifts the eightfold degeneracy of

the Yb³⁺ moments, producing a Kramers doublet ground state that is a nearly pure state of the total angular momentum, $J, |J, m_J\rangle = |7/2, \pm 7/2\rangle$. The estimated anisotropy of the Landé *g* factor is in good agreement with that of the measured magnetization, $g_{\parallel}/g_{\perp} = 7.5(4)$ (4–7), implying strong Ising anisotropy in Yb₂Pt₂Pb, which confines the individual Yb moments to two orthogonal sublattices in the *ab* plane.

The quantum states of the $|\pm 7/2\rangle$ Ising doublet are the superpositions of its “up” and “down” components, $\alpha_{\uparrow}|7/2\rangle + \alpha_{\downarrow}|-7/2\rangle$, and therefore the doublet can be viewed as an effective quantum spin-1/2. However, familiar interactions like the Zeeman, Heisenberg-Dirac exchange, and dipole interactions that are bilinear in *J* can only change the total angular momentum quantum number by $\Delta m_J = \pm 1$; they have no matrix elements that would allow transitions between the moment-reversed states of the ground state wave function. Only multiple virtual processes involving excited states could reverse individual Yb moments, but these processes are expected to be very weak because the ground and first excited states are separated by as much as 25 meV, according to specific heat (4) and inelastic neutron-scattering measurements (6). This would suggest that Yb₂Pt₂Pb would display only static, classical Ising behavior, but our data are not consistent with this picture.

Here we report neutron-scattering experiments on Yb₂Pt₂Pb that reveal a continuum of low-energy quantum excitations that display the distinctive spinon dispersion along the *c* axis (Fig. 2A), typical of the $S = 1/2$ Heisenberg-Ising XXZ spin Hamiltonian (8),

$$H = J \sum_n (S_n^x S_{n+1}^x + S_n^y S_{n+1}^y + \Delta S_n^z S_{n+1}^z) \quad (1)$$

where *J* is the Heisenberg spin-exchange coupling and Δ is its anisotropy. This observation provides definitive evidence that the Yb moments in Yb₂Pt₂Pb behave as quantum-mechanical spins-1/2 (9). The spinon spectrum $M(\mathbf{Q}, E)$ is fully gapped, but the gap is much smaller than the excitation bandwidth, indicating only moderate Ising anisotropy, $\Delta \gtrsim 1$. The lack of any wave

¹Department of Physics and Astronomy, Stony Brook University, Stony Brook, NY 11794, USA. ²Condensed Matter Physics and Materials Science Division, Brookhaven National Laboratory, Upton, NY 11973, USA. ³Quantum Condensed Matter Division, Oak Ridge National Laboratory, Oak Ridge, TN 37831, USA. ⁴Department of Physics and Astronomy, Texas A&M University, College Station, TX 77843, USA. ⁵Max Planck Institute for the Physics of Complex Systems, Nöthnitzer Strasse 38, 01187 Dresden, Germany. ⁶Institute for Theoretical Physics, University of Amsterdam, Science Park 904, 1098 XH Amsterdam, Netherlands. ⁷NIST Center for Neutron Research, National Institute of Standards and Technology, Gaithersburg, MD 20899, USA. *Corresponding author. Email: zaliznyak@bnl.gov

vector Q_{HH} dispersion for this gap (Fig. 2B), or for the scattering intensity in the ab plane (Fig. 2C), indicates that the dispersing excitations are confined to the ladder rails, which form an array of weakly coupled spin-1/2 chains.

The overall wave vector dependence of the energy-integrated intensity $M(Q)$ (Fig. 2, C and D) reveals that the excitations in each of the two orthogonal sublattices of Yb moments in $\text{Yb}_2\text{Pt}_2\text{Pb}$ are longitudinally polarized. This is clearly dem-

onstrated in Fig. 2D, where the $M(Q)$ dependence on H in the (H, H, L) scattering plane is very accurately described by the projections of Yb moments on the wave vector, consistent with the polarization factor in the neutron-scattering cross-section, which is only sensitive to magnetic fluctuations perpendicular to Q . The longitudinal character of magnetic excitations in $\text{Yb}_2\text{Pt}_2\text{Pb}$ is a direct consequence of the strong orbital anisotropy imposed by the crystal field and the resulting strongly anisotropic Landé g -factor. Even if the effective spin Hamiltonian that describes the low-energy dynamics in $\text{Yb}_2\text{Pt}_2\text{Pb}$ has modes involving transverse spin fluctuations, such as spin waves, they virtually do not couple to physical fields at our disposal and are de facto invisible in experiments. In particular, the measured longitudinal spectrum, which is typical of a spin-1/2 XXZ chain (Fig. 2), indicates the presence of transverse spinon excitations (8, 10–12), but these are not seen in experiments. That the XY-part of the effective spin Hamiltonian Eq. 1 is unobservable results from the well-understood effect of quantum selection rules. The direct consequence for our measurements is that we do not observe a (transverse) magnon, which is expected (13) when a magnetic field $B = 4$ T applied along (1-10) crystal direction saturates Yb moments that are parallel to the field (4–7), bringing this sublattice to the ferromagnetic (FM) state (Fig. 1B). Instead, FM chains do not contribute to magnetic scattering, and this allows us to use the 4 T data as a background that can isolate their contribution at $B = 0$ (Fig. 2D).

To establish the hierarchy of energy scales in the effective $S = 1/2$ XXZ Hamiltonian, we fit the energy cuts at different values of Q_L to a phenomenological half-Lorentzian line shape (14), which accounts both for the sharp continuum onset and its broad, asymmetric extent to higher energies (Fig. 3, A and B). We can thus very accurately determine the lower boundary, $E_L(Q_L)$, of the spinon continuum (points in Fig. 2A), which we fit to the exact Bethe-Ansatz expression for the XXZ Hamiltonian (Eq. 1) (8, 10, 11),

$$E_L(Q_L) = \min\{\Delta_s + \varepsilon_s(Q_L), 2\varepsilon_s(Q_L/2)\},$$

$$\varepsilon_s(Q_L) = \sqrt{I^2 \sin^2(\pi Q_L) + \Delta_s^2 \cos^2(\pi Q_L)} \quad (2)$$

Here Δ_s is the gap and I the bandwidth of the spinon dispersion, $\varepsilon_s(Q_L)$, both of which are functions of the J and Δ parameters of the Hamiltonian Eq. 1 (6). The fit yields values $I = 0.322(20)$ meV and $\Delta_s = 0.095(10)$ meV for the spinon dispersion parameters, which correspond to $\Delta \approx 3.46$, and $J = 0.116(10)$ meV in the effective spin-1/2 XXZ Hamiltonian, and the excitation gap at $Q_L = 1$, $E_g = 2\Delta_s = 0.19(2)$ meV. Despite the strong anisotropy of the individual Yb moments, their inferred coupling in the spin chain is surprisingly close to the isotropic Heisenberg limit $\Delta = 1$, as evidenced by the smallness of the excitation gap E_g compared to their observed bandwidth $\gtrsim 1$ meV (Fig. 2A).

Computations carried out on the XXZ Hamiltonian Eq. 1 closely reproduce key aspects of

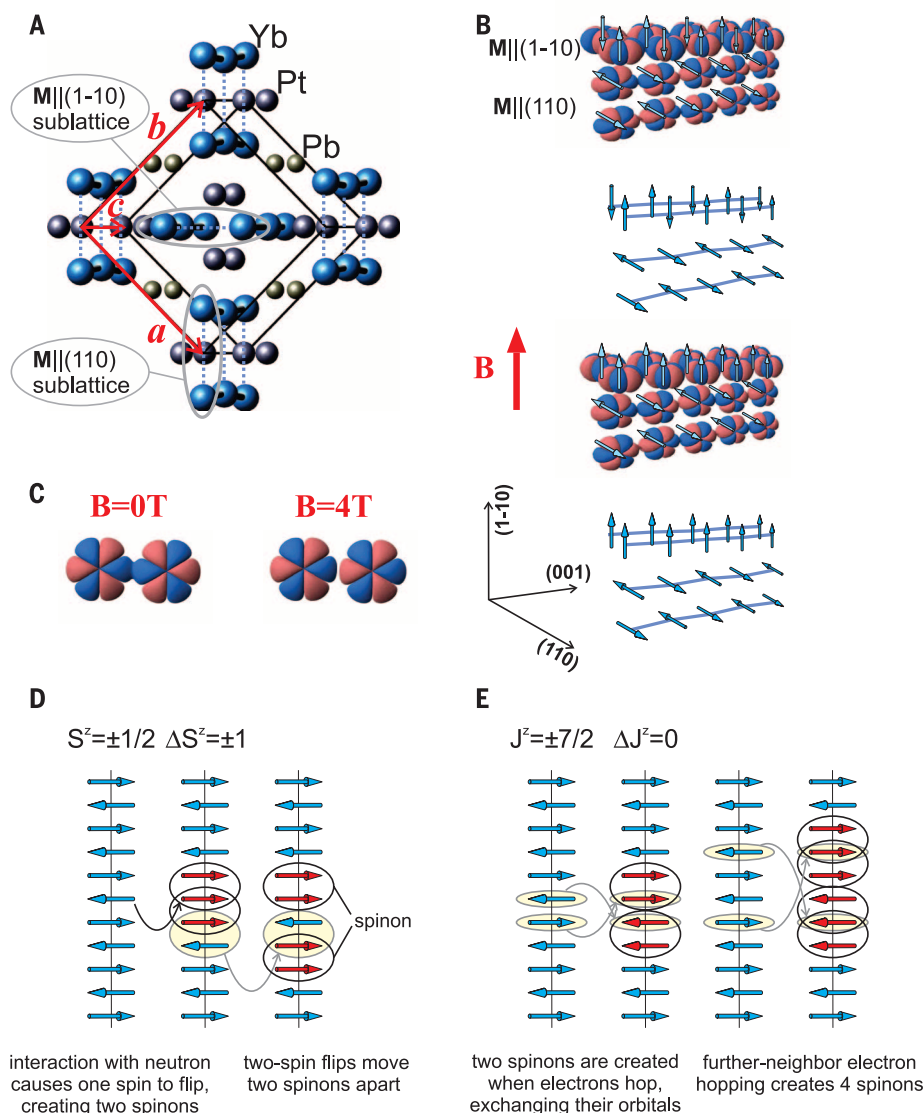


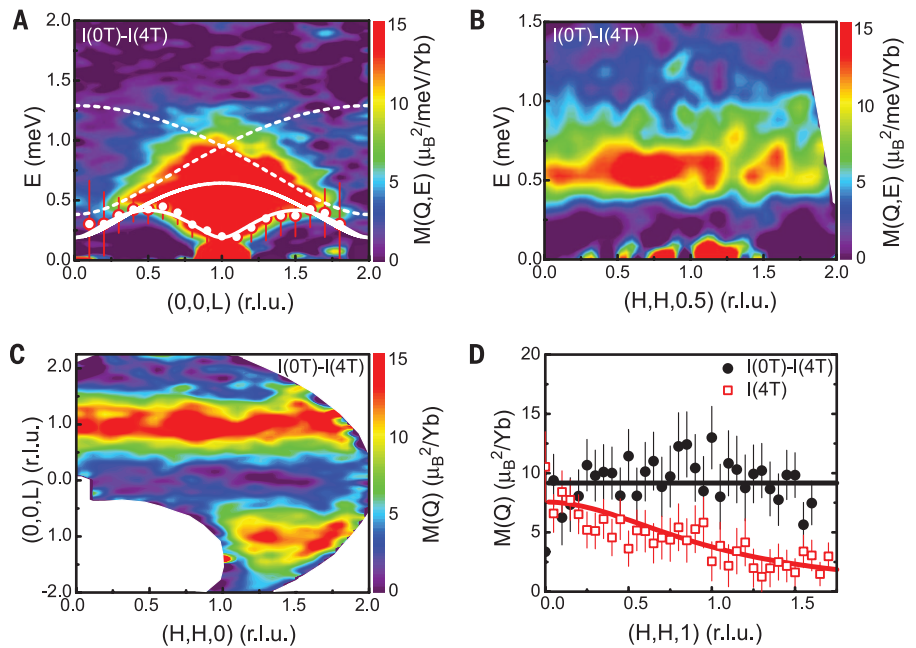
Fig. 1. Quantum orbital-spin chains in $\text{Yb}_2\text{Pt}_2\text{Pb}$. (A) Crystal structure of $\text{Yb}_2\text{Pt}_2\text{Pb}$; red arrows show the lattice axes. (B) The double chain magnetic structure for $T < T_N = 2.07$ K without magnetic field (top) and in a 4 T field applied along the (1-10) direction (bottom). The Yb orbitals are depicted as the isosurfaces, at 1 part per million electronic density, of the $4f |m_L| = 3$ hydrogenic wave functions for an effective Slater nuclear charge of ^{70}Yb (29). Blue arrows indicate the ordered magnetic moment directions, which are parallel to the local Ising easy axes, horizontal for the (110) and vertical for the (1-10) sublattice. Crystal axes are shown by black arrows. Thick red arrow shows magnetic-field direction. (C) Orbital overlaps for antiferromagnetic ($B = 0$) and fully saturated ($B = 4$ T) state. (D) Illustration of the two-spinon excitation process via spin flip (magnon) creation in $S = 1/2$ antiferromagnetic chain. Such processes correspond to the change of angular momentum, $\Delta m_S \equiv \Delta S^z = \pm 1$, and are allowed by selection rules that govern interaction with a physical field, such as magnetic field of a neutron, or a photon. (E) For $m_J = J^z = \pm 7/2$, angular momenta in $\text{Yb}_2\text{Pt}_2\text{Pb}$, flipping magnetic moment requires $\Delta m_J = \pm 7$ and therefore cannot be induced via single-particle processes. The only processes allowed by the selection rules are those with $\Delta m_J = 0$, such as when two electrons hop, exchanging their orbitals, i.e., pairwise permutations of electrons. Permutation of two nearest-neighbor electrons creates two spinons, while further-neighbor hopping, such as the permutation of the next-nearest-neighbor electrons in opposite-polarity orbitals illustrated in the figure, results in a four-spinon state.

Fig. 2. Fractional spinon excitations in Yb₂Pt₂Pb.

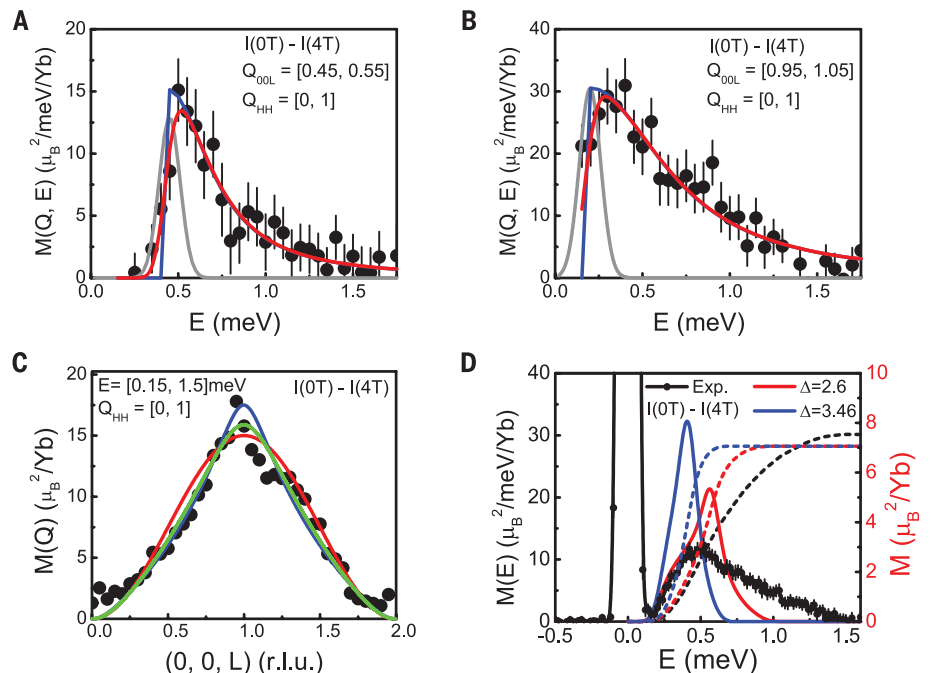
(A) The dispersion of the spectrum of magnetic excitations along the Q_L direction in reciprocal space of Yb₂Pt₂Pb at $T = 0.1$ K, obtained by averaging the scattered neutron intensity over the first Brillouin zone in Q_{HH} , along the perpendicular, $(H, H, 0)$ direction. Circles: onset of the excitation continuum determined by fitting the constant- Q_L data. Solid white lines: lower and upper boundaries of the two-spinon continua. Dashed lines: upper boundaries of the four-spinon continua (6). (B) The dispersion of the scattered neutron intensity along the Q_{HH} direction for $Q_L = 0.5 \pm 0.1$. (C) The partial static structure factor, $M(\mathbf{Q})$, obtained by integrating the scattered intensity from 0.15 to 1.5 meV. $M(\mathbf{Q})$ depends on the relative orientation of the scattering vector $\mathbf{Q} = (H, H, L)$ and the direction of magnetic moment fluctuations (30). (D) At 4 T, $M(\mathbf{Q})$ (red squares) follows the projection of the (110) sublattice moments on the scattering wave

vector (polarization factor $P(4T) = \frac{(Lc^*)^2}{2(Ha^*)^2 + (Lc^*)^2}$, red line), indicating that only magnetic fluctuations along the (110) moments contribute to magnetic scattering. Both polarizations are present when $B = 0$ T, consistent with equal longitudinal spinon spectral

weight in both (110) and (1-10) sublattices. By subtracting the 4 T data from the 0 T data (black dots), we can isolate the scattering from fluctuations along the field direction, (1-10), which are always perpendicular to the scattering vector \mathbf{Q} and whose polarization factor is constant (black line). The agreement between the polarization factors and our data confirms that only fluctuations of the Yb moments that lie along the respective (110) or (1-10) direction are seen in our experiment and that there is no measurable transverse component of magnetic moment or excitations. Error bars in all figures represent 1 SD.

**Fig. 3. Spinon line shapes and the onset of the continuum in Yb₂Pt₂Pb.**

The spectrum of the dynamical structure factor of magnetization fluctuations, $M(\mathbf{Q}, E)$, in Yb₂Pt₂Pb for (A) $Q_L = 0.50(5)$ ($q_{\text{chain}} = \pi/2$) and (B) $Q_L = 1.00(5)$ ($q_{\text{chain}} = \pi$), both integrated within 1 Brillouin zone in Q_{HH} . The red lines show fits to the “half-Lorentzian” line shape (blue) convoluted with the Gaussian of 0.1 meV full width at half-maximum representing the resolution of the DCS spectrometer (light gray), (14). (C) The energy-integrated scattering function $M(\mathbf{Q})$ obtained by summing the normalized data over the first Brillouin zone in Q_{HH} compares favorably with that calculated for the effective $S = 1/2$ Heisenberg-Ising Hamiltonian with $\Delta = 2.6$ and $J = 0.205$ meV and with the effective g -factor $g^{\text{eff}} \approx 10$ (blue line), and with $\Delta = 3.46$, $J = 0.116$ meV, and $g^{\text{eff}} \approx 13$ (green line). A fit to the leading Ising-limit ($\Delta \gg 1$) expression, $M(\mathbf{Q}) = \frac{(g^{\text{eff}}\mu_B)^2}{2\Delta^2} \sin^2(\frac{\pi Q_L}{2})$, (red line) is less satisfactory, emphasizing that effective spin-1/2 Hamiltonian in Yb₂Pt₂Pb is not extremely Ising-like. This is consistent with the observation that the gap in the spinon spectrum, $E_g \approx 0.19$ meV (B), is markedly smaller than the bandwidth, ≥ 1 meV, Fig. 2A. (D) The energy dependence of the \mathbf{Q} -integrated intensity, which represents the local dynamical structure factor, $M(E)$, of magnetization fluctuations in Yb₂Pt₂Pb. The energy-integral of the $M(E)$ inelastic intensity (black dashed line, right scale) gives the square of the total fluctuating magnetic moment of $\approx 7.6\mu_B^2$ per Yb. Computational results for $M(E)$ and its energy integral are compared for $\Delta = 2.6$ (red solid and dashed lines) and $\Delta = 3.46$ (blue solid and dashed lines).



our experimental results. The mixed Heisenberg-Ising character of Yb₂Pt₂Pb is evident in the broad peak at $Q_L = 1$ in the structure factor $M(\mathbf{Q})$ found by integrating the experimental and computed spectra in energy (Fig. 3C). $M(\mathbf{Q})$ is inter-

mediate between the near divergence expected for isotropic interactions ($\Delta = 1$) and the leading-order Ising expression (15) $M(\mathbf{Q}) = 2M_0^2 \frac{1}{\Delta^2} \sin^2(\frac{\pi Q_L}{2})$, where $M_0 = \frac{1}{2}g_{\parallel}^{\text{eff}}\mu_B$ is Yb magnetic moment, $g_{\parallel}^{\text{eff}}$ being the effective spin-1/2 g -factor for the local

Ising direction. Crystal electric field calculations for the Yb ground state doublet in Yb₂Pt₂Pb indicate $g_{\parallel}^{\text{eff}} = 7.9$ and $g_{\perp}^{\text{eff}} \leq 0.8$ (6), so that magnetic neutron-scattering intensity, which is proportional to $(g_{\parallel}^{\text{eff}})^2$, is at least a factor of 100 weaker

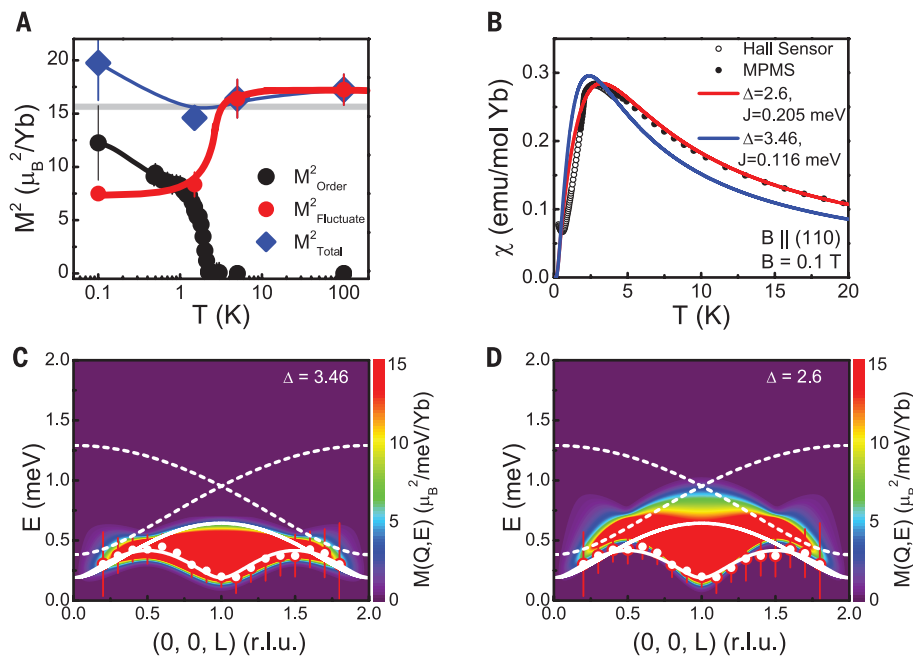


Fig. 4. Spinons in $\text{Yb}_2\text{Pt}_2\text{Pb}$: theory and experiment. (A) Temperature dependencies of the ordered Yb moment from neutron-diffraction measurements (black circles), the fluctuating moment from the energy and wave-vector integrated normalized $M(Q, E)$ (red points), and the total (blue points). (B) The temperature dependence of the static, uniform magnetic susceptibility $\chi(T)$ for $\text{Yb}_2\text{Pt}_2\text{Pb}$ (black circles), measured with a magnetic properties measurement system ($T \geq 1.8 \text{ K}$) and a Hall sensor magnetometer ($0.2 \text{ K} \leq T \leq 4 \text{ K}$), shows good agreement with $\chi(T)$ calculated for the XXZ chain, for $\Delta = 2.6$ and $J = 0.205 \text{ meV}$ (red line, $g^{\text{eff}} \approx 7.4$). Agreement is less good for $\Delta = 3.46$ and $J = 0.116 \text{ meV}$ (blue line, $g^{\text{eff}} \approx 6.5$). (C and D) The longitudinal structure factor, $M(Q, E)$, of the XXZ spin-1/2 chain Eq. 1 calculated using the algebraic Bethe ansatz (11, 12, 20) (C) for $\Delta = 3.46$ and $J = 0.116 \text{ meV}$ and (D) for $\Delta = 2.6$ and $J = 0.205 \text{ meV}$. The experimentally determined lower boundary $E_L(Q_L)$ is shown (circles) along with the calculated lower and upper two-spinon (solid lines) and the upper four-spinon (broken lines) boundaries, as described in the text. The calculation is normalized to the total experimental intensity by using the sum rule for a single component of the dynamical structure factor, which holds for spin-1/2, $\iint S^Z(Q, E) \frac{dQ}{2\pi} dE = \frac{1}{4}$.

for the transverse, XY-polarized fluctuations, in agreement with what we observe.

The Q -integrated scattering in Fig. 3C yields a fluctuating moment $M^2_{\text{fluct}} \approx 7.1\mu_B^2/\text{Yb}$ at 0.1 K, about half as large as the ordered moment M^2_{order} determined in previous work (16). The energy integral of the local autocorrelation function $M(E)$, which is obtained by integrating the measured intensity in Q , yields a similar result, $\approx 7.6\mu_B^2/\text{Yb}$ (Fig. 3D), with the difference indicating a systematic error resulting from different data binning. The sum rule for the effective spin-1/2 dictates that the integral intensity in each polarization channel is $(S^\alpha)^2 = 1/4$ ($\alpha = x, y, z$). Therefore, the sum $M^2_{\text{fluct}} + M^2_{\text{order}}$ gives a total Yb moment, $M^2_{\text{total}} = (\frac{1}{2}g^{\text{eff}}\mu_B)^2$. Combining the inelastic spectrum and the elastic order parameter measurements in $\text{Yb}_2\text{Pt}_2\text{Pb}$ (6), we find M_{total} that is between 3.8 and 4.4 μ_B/Yb [$g^{\text{eff}} = 8.2(5)$] for temperatures from 0.1 to 100 K (Fig. 4A), fully consistent with the predictions of the point charge model. The spinons provide virtually all of the magnetic dynamics in $\text{Yb}_2\text{Pt}_2\text{Pb}$, and they are completely captured by our experiments. This result immediately rules out a naïve explanation that the observed longitudinal magnetic response

could originate from the two-magnon continuum, as in conventional magnets, because in that case the continuum would comprise only a small part of the dynamical spectral weight (17, 18). Moreover, stable magnons do not exist in an antiferromagnetic spin-1/2 chain, where the elementary excitations are spinons, and the system's one-dimensionality is clearly established by the measured dispersion (Fig. 2, A to C). Finally, the static spin susceptibility $\chi_s(T)$ computed for spin-1/2 XXZ chain with $g^{\text{eff}} \approx 7$ closely reproduces direct measurements of $\chi(T)$ (Fig. 4B).

Further comparison with the exact result (19) for the XXZ model (Eq. 1), however, indicates that the fluctuations measured in $\text{Yb}_2\text{Pt}_2\text{Pb}$ at 0.1 K are stronger than the predicted spinon contribution to the dynamical spin structure factor, which for $\Delta = 3.46$ is only $\approx 20\%$ of the ordered spin contribution S^2_{order} . Figure 3D makes it clear that the calculated $M(E)$ underestimates the contribution of the high-energy states in $\text{Yb}_2\text{Pt}_2\text{Pb}$. Direct comparison of the detailed energy dependencies of the measured (Fig. 2A) and computed (broadened by the instrumental resolution of 0.1 meV) (Fig. 4C) spectra of longitudinal excitations reveals that there is considerable spectral weight

present in the experimental data above the upper boundary of the two-spinon continuum, $E_U(Q_L) = \max\{\Delta_s + \epsilon_s(Q_L), 2\epsilon_s(Q_L/2)\}$, that is absent in the computed spectrum (10, 11). A somewhat better agreement can be obtained by fitting the measured intensity to the calculated longitudinal structure factor $M(Q, E)$ and adjusting Δ and J as fit parameters instead of adopting the values determined from the lower boundary of the continuum. This results in $\Delta = 2.6$ and $J = 0.205 \text{ meV}$ (Fig. 4D), shifting the two-spinon spectral weight to higher energy and also providing better agreement with the measured susceptibility (Fig. 4B) and $M(Q)$ (Fig. 3C). However, this improvement is achieved at the cost of the excellent experimental and theoretical agreement for the lower spinon boundary, which, in fact, is determined very precisely from the line fits (Fig. 3, A and B). This dilemma is resolved by noting that the observed high-energy magnetic spectral weight in $\text{Yb}_2\text{Pt}_2\text{Pb}$ is consistent with a substantial contribution of four-spinon states, whose upper boundaries (12) are shown by the broken lines in Fig. 2A. This result is quite unexpected, given that two-spinon excitations account for all but a few percent of the total spectral weight (12, 13, 20) in the nearest-neighbor Heisenberg-Ising chain.

We now show that these seemingly perplexing experimental results can be understood in terms of the interplay of 4f-electron exchange, strong spin-orbit coupling, and a crystal field that lifts the large orbital degeneracy of the $J = 7/2$ multiplet. The intersite electron hopping in the f-electron Hamiltonian for $\text{Yb}_2\text{Pt}_2\text{Pb}$, which we adopt in the form of a 1D Hubbard model (6), leads to an electronic interaction (21) whose physical nature is not a Heisenberg-Dirac spin exchange (1, 2), but rather an orbital exchange (Fig. 1), a realization that has been appreciated in the physics of Kondo effect (22, 23) and more recently in certain cold-atom systems (24).

The orbital-exchange interaction in $\text{Yb}_2\text{Pt}_2\text{Pb}$ is a natural generalization of the Heisenberg-Dirac spin exchange between the two electrons, and has the same physical origin in the electronic Coulomb repulsion (1, 2). The magnetism in $\text{Yb}_2\text{Pt}_2\text{Pb}$ is tied to the wave function of a single 4f hole with orbital momentum $L = 3$, $|m_L| = 3$, having sixfold symmetry around the J quantization axis, given by the magnetic structure as perpendicular to the rails of Yb ladders in $\text{Yb}_2\text{Pt}_2\text{Pb}$ crystal. The energy cost for hopping between sites, which in $\text{Yb}_2\text{Pt}_2\text{Pb}$ is synonymous with orbital exchange, is reduced when neighboring Yb ions are in alternating states of $m_L = \pm 3$, because in that case, the exchange of electrons between the two sites required for hopping involves the overlap of two identical orbital lobes along the ladder rails (Fig. 1, B and C). The sixfold symmetry of the f-orbital breaks the rail-rung equivalence and ensures that this energy advantage is not accrued for hopping in a transverse direction, decoupling the ladder rails. Combined with the weak interactions between orthogonal ladders mandated by the SSL geometry (4), this leads to the spin-chain nature of the emergent effective Hamiltonian.

The leading-order Coulomb contribution for the low-energy manifold of electronic states ($6, 25$) is given by the two-electron permutation operator, P_{12} , which in the cases where only electronic spins are at play, reduces to the usual Heisenberg spin exchange, $\sim S_1 S_2$. For the case of a J -manifold, which in the absence of crystal fields is highly degenerate, it has the form of a permutation operator acting on a $(2J + 1) \times (2J + 1)$ -dimensional space of two neighboring Yb ions. The permutation operator interchanges states $|m_{j1}, m_{j2}\rangle$ and $|m_{j2}, m_{j1}\rangle$ with equal weights, thus including the process $|7/2, -7/2\rangle$ to $|-7/2, 7/2\rangle$ where both moments simultaneously reverse, which cannot be achieved through conventional Heisenberg-Dirac spin exchange (Fig. 1, D and E). The crystal field lifts the degeneracy of the Yb moments, and although the effective interaction that emerges after the projection on the manifold of the lowest Kramers doublets $m_j = \pm 7/2$ has the form of the antiferromagnetic $S = 1/2$ XXZ Hamiltonian, it retains the birthmark of its unusual origin in exchange processes that are distinct from those having the conventional Heisenberg $J_1 J_2$ form.

The effective spin-1/2 physics emerges in $\text{Yb}_2\text{Pt}_2\text{Pb}$ from the combination of high-energy (Coulomb, spin-orbit, hopping) interactions. The spin-orbit coupling virtually quenches the electronic spin degree of freedom, forcing its alignment with the large orbital moment, and in this way the effective spin-1/2 XXZ model effectively describes the quantum dynamics of the electronic orbital degree of freedom. This is directly evidenced in our experiments by the large, $\approx 4\mu_B$ magnetic moment carried by spinons. The orbital exchange sets the scale for these emergent quantum dynamics, which we find by comparing the measured spinon dispersion with computed spectra (Fig. 4).

Because the orbital angular momentum dominates the total Yb moment, magnetic order in $\text{Yb}_2\text{Pt}_2\text{Pb}$ is synonymous with orbital order, and the configuration depicted in Fig. 1, D and E, is a natural way to understand how permutation of two neighboring electrons generates two spinons in the antiferromagnetic background. This is a process that entails charge-orbital separation, because the electron count per site is unchanged by correlated hopping, but the phases of the orbital wave function on both sites are reversed. Further-neighbor orbital exchange leads to states with four spinons (Fig. 1E). Hence, long-range hopping, either by virtue of the in-chain itinerancy of the 4f electrons or via coupling to the conduction electrons in metallic $\text{Yb}_2\text{Pt}_2\text{Pb}$, provides a natural mechanism for the spectral weight of the excitations that we observe above the two-spinon but within the four-spinon continuum boundaries.

Our results provide a specific mechanism for charge-orbital separation in $\text{Yb}_2\text{Pt}_2\text{Pb}$, where the proliferation of spinons implies that electrons lose their orbital-phase identity. When united with the previous demonstrations of spin-charge and spin-orbital separation, this finding completes the triad of electron fractionalization phenomena in one dimension (26–28).

REFERENCES AND NOTES

- W. Heisenberg, *Z. Phys.* **49**, 619–636 (1928).
- P. A. M. Dirac, *Proc. R. Soc. London, A Contain. Pap. Math. Phys. Character* **123**, 714–733 (1929).
- B. S. Shastry, B. Sutherland, *Physica B+C* **108**, 1069–1070 (1981).
- M. S. Kim, M. C. Bennett, M. C. Aronson, *Phys. Rev. B* **77**, 144425 (2008).
- M. S. Kim, M. C. Aronson, *Phys. Rev. Lett.* **110**, 017201 (2013).
- See supplementary materials on Science Online for details.
- A. Ochiai et al., *J. Phys. Soc. Jpn.* **80**, 123705 (2011).
- H. A. Bethe, *Z. Phys.* **71**, 205–226 (1931).
- L. Faddeev, L. Takhtajan, *Phys. Lett. A* **85**, 375–377 (1981).
- A. H. Bougourzi, M. Karbach, G. Müller, *Phys. Rev. B* **57**, 11429–11438 (1998).
- J.-S. Caux, J. Mossel, I. P. Castillo, *J. Stat. Mech.* **2008**, P08006 (2008).
- J.-S. Caux, R. Hagemans, *J. Stat. Mech.* **2006**, P12013 (2006).
- M. Mourigal et al., *Nat. Phys.* **9**, 435–441 (2013).
- I. A. Zaliznyak, S.-H. Lee, S. V. Petrov, *Phys. Rev. Lett.* **87**, 017202 (2001).
- N. Ishimura, H. Shiba, *Prog. Theor. Phys.* **63**, 743–758 (1980).
- W. Müller et al., *Phys. Rev. B* **93**, 104419 (2016).
- D. A. Tennant et al., *Phys. Rev. B* **67**, 054414 (2003).
- T. Huberman et al., *Phys. Rev. B* **72**, 014413 (2005).
- R. Baxter, *J. Stat. Phys.* **9**, 145–182 (1973).
- A. C. Walters et al., *Nat. Phys.* **5**, 867–872 (2009).
- K. I. Kugel, D. I. Khomskii, *Sov. Phys. JETP* **37**, 725 (1973).
- B. Coqblin, J. R. Schrieffer, *Phys. Rev.* **185**, 847–853 (1969).
- P. Coleman, *Phys. Rev. B* **28**, 5255–5262 (1983).
- A. V. Gorshkov et al., *Nat. Phys.* **6**, 289–295 (2010).
- G. Uimin, Y. Kudasov, P. Fulde, A. Ovchinnikov, *Eur. Phys. J. B* **16**, 241–244 (2000).
- B. J. Kim et al., *Nat. Phys.* **2**, 397–401 (2006).
- J. Schlappa et al., *Nature* **485**, 82–85 (2012).
- P. W. Anderson, *Phys. Today* **50**, 42 (1997).
- J. C. Slater, *Phys. Rev.* **36**, 57–64 (1930).
- G. L. Squires, *Introduction to the Theory of Thermal Neutron Scattering* (Cambridge Univ. Press, UK, ed. 3, 2012).

ACKNOWLEDGMENTS

Work at Brookhaven National Laboratory (I.A.Z., A.M.T., M.S.K.) was supported by the Office of Basic Energy Sciences (BES), Division of Materials Sciences and Engineering, U.S. Department of Energy (DOE), under contract DE-SC00112704. Work at Stony Brook (L.S.W., W.J.G., M.C.A.) was supported by NSF-DMR-1310008. L.S.W. was also supported by the Laboratory Directed Research and Development Program of Oak Ridge National Laboratory (ORNL). This research at ORNL's Spallation Neutron Source was sponsored by the Scientific User Facilities Division, Office of Basic Energy Sciences, U.S. DOE. Work at NIST Center for Neutron Research (NCNR) is supported in part by the NSF under Agreement no. DMR-1508249. J.-S.C. and M.B. acknowledge support from the Netherlands Organization for Scientific Research (NWO) and the Foundation for Fundamental Research on Matter (FOM) of the Netherlands.

SUPPLEMENTARY MATERIALS

www.sciencemag.org/content/352/6290/1206/suppl/DC1
Materials and Methods
Supplementary Text
Figs. S1 to S10
Tables S1 to S3
References (31–53)

17 December 2015; accepted 29 April 2016
10.1126/science.aaf0981

Orbital-exchange and fractional quantum number excitations in an f-electron metal, Yb₂Pt₂Pb

L. S. Wu, W. J. Gannon, I. A. Zaliznyak, A. M. Tsvelik, M. Brockmann, J.-S. Caux, M. S. Kim, Y. Qiu, J. R. D. Copley, G. Ehlers, A. Podlesnyak and M. C. Aronson (June 2, 2016)
Science **352** (6290), 1206-1210. [doi: 10.1126/science.aaf0981]

Editor's Summary

Orbitals and charge go their separate ways

In certain materials at very low temperatures, an electron's spin can separate from its charge, zooming through the crystal in the form of a "spinon." Such materials are usually one-dimensional, and their atoms have spins of 1/2. Wu *et al.* observed related behavior in a three-dimensional metal, Yb₂Pt₂Pb, where the Yb ions have a large magnetic moment that has its origin in the electrons' orbital motion rather than their spin. Neutron-scattering measurements indicated that these large magnetic moments can flip their direction through an exchange process similar to the one that occurs in spin 1/2 systems. This process results in effective charge-orbital separation.

Science, this issue p. 1206

This copy is for your personal, non-commercial use only.

Article Tools Visit the online version of this article to access the personalization and article tools:
<http://science.sciencemag.org/content/352/6290/1206>

Permissions Obtain information about reproducing this article:
<http://www.sciencemag.org/about/permissions.dtl>

Science (print ISSN 0036-8075; online ISSN 1095-9203) is published weekly, except the last week in December, by the American Association for the Advancement of Science, 1200 New York Avenue NW, Washington, DC 20005. Copyright 2016 by the American Association for the Advancement of Science; all rights reserved. The title *Science* is a registered trademark of AAAS.